A CIRCUMFERENTIAL SLOT VIRTUAL IMPACTOR FOR BIOAEROSOL CONCENTRATION

A Thesis

by

CLINTON WAYNE ADAMS

Submitted to the Office of Graduate Studies of
Texas A&M University
in partial fulfillment of the requirements for the degree of

MASTER OF SCIENCE

December 2006

Major Subject: Mechanical Engineering

A CIRCUMFERENTIAL SLOT VIRTUAL IMPACTOR FOR BIOAEROSOL CONCENTRATION

A Thesis

by

CLINTON WAYNE ADAMS

Submitted to the Office of Graduate Studies of
Texas A&M University
in partial fulfillment of the requirements for the degree of

MASTER OF SCIENCE

Approved by:

Chair of Committee, Andrew McFarland
Committee Members, John Haglund
Yassin Hassan
Head of Department, Dennis O'Neal

December 2006

Major Subject: Mechanical Engineering

ABSTRACT

A Circumferential Slot Virtual Impactor for Bioaerosol Concentration. (December 2006)

Clinton Wayne Adams, B.S., Texas A&M University

Chair of Advisory Committee: Dr. Andrew McFarland

A virtual impactor aerosol concentrator with a circumferential inlet slot has been built and tested. Circumferential slot virtual impactors (CSVIs) have low pressure losses, similar to linear slot impactors, but without particle losses due to end effects.

The CSVI was designed using the results from a computational fluid dynamics study. The device has a total sampling flow rate of 10 to 30 L/min and a concentration factor of 10:1. CSVIs were built based on the CFD study design and tested with oleic acid droplets and polystyrene latex beads. The test results found a cutpoint Stokes number of 0.75 and 90% particle transmission at least 52X the Stokes cutpoint. At a flow rate of 10 L/min the cutpoint is 2.0 µm aerodynamic diameter (AD) and >90% transmission efficiency was found between 4 µm AD, and 22 µm AD. At the flow rate of 30 L/min the cutpoint is 1.2 µm AD and a >90% transmission efficiency was found between 2 and 10 µm AD. Performance and pressure drop curves were found for a variety of flow rates. The pressure drop across the CSVI at 10 L/min was 270 Pa (1.1 in H_2O) with an ideal power consumption of 0.045 watts. At 30 L/min the pressure drop was 970 Pa (3.9 in H_2O) with an ideal power consumption of 0.44 watts.

ACKNOWLEDGEMENTS

Funding for this study was provided by the U.S. Army Research, Development, and Engineering Command (RDECOM), Edgewood Chemical Biological Center (ECBC), under the supervision of Dr. Edward Steubing and Dr. Jerry Bottiger (Texas Engineering Experiment Station, Contract Number 32579-60240.) I would like to extend a heartfelt thank you to my advisor, Dr. Andrew McFarland, for his guidance throughout my studies. I am also grateful to my committee members and all of my colleges at the Aerosol Technology Laboratory, especially those who worked with me directly on this project: Dr. John Haglund, Gary Bradley, Daniel Lacrioux, and John Vaughan.

A special thank you goes to Sridhar Hari, Shishan Hu, and Satya Sheshadri. The numerical work that they contributed to this project was pivotal in making it a success.

NOMENCLATURE

C_c	=	Cunningham correction factor (for particle slip)
C_m	=	Concentration of aerosol of diameter (D_p) in the minor flow
C_{vol}	=	Volume fraction of oleic acid and fluorescein
C_∞	=	Concentration of aerosol of a particular diameter in the ambient air
D_c	=	Diameter of the fractionation zone
D_p	=	Particle diameter
F_s	=	Fluorometer reading from an experimental sample
F_r	=	Fluorometer reading of a reference sample
f_{VOAG}	=	Vibrating orifice aerosol generator excitation frequency
Ki	=	The minor loss coefficient for a passage in the CSVI
L_c	=	Fractionation zone characteristic dimension
P_{meas}	=	Measured particle penetration from experimentation
Q_i	=	Flow rate through a passage in the CSVI
Q_{maj}	=	Flow rate through the major flow passages in the CSVI
Q_{min}	=	Flow rate through the minor flow passage in the CSVI
Q_s	=	Total flow rate through the CSVI
Q_r	=	Flow rate through the reference filter
Q_{VOAG}	=	Solution flow rate through the Vibrating Orifice Aerosol Generator
R	=	Dynamic range
Re	=	Reynolds number

Stk	=	Stokes number
Stk_{50}	=	Stokes cutpoint
$Stk_{90_{UB}}$	=	Upper bound Stokes 90
$Stk_{90_{LB}}$	=	Lower bound Stokes 90
TE	=	Particle penetration
t_s	=	CSVI aerosol sampling interval
t_r	=	Reference filter sampling interval
V_s	=	Volume of the solvent added to experimental filters
V_r	=	Volume of the solvent added to reference filters
x_{fr}	=	Fraction of ethanol in master solution
X_i	=	Variable used in the calculation of R (used in uncertainty calculation)
U_0	=	Mean air velocity at the acceleration exit plane
V_d	=	Volume of dilution ethanol
V_m	=	Volume of master solution
w	=	Width of the accelerator nozzle nozzle
$\dot{W}_{Ideal}$	=	Ideal power consumption of the CSVI
δX_i	=	Uncertainty of a variable X_i
ΔP_i	=	Pressure drop across passage in the CSVI
ΔP_{maj}	=	The average pressure drop across the major flow passage in the CSVI
ΔP_{min}	=	The pressure drop across the minor flow passage in the CSVI
λ	=	Particle mean free path in air

μ = Air viscosity

ρ_f = Density of air

ρ_p = Particle density

TABLE OF CONTENTS

Page

Page

LIST OF FIGURES

Page

LIST OF TABLES

Page

INTRODUCTION

General

With recent events, the threat of terrorism to the United States was made apparent. One of the most highly discussed of the terrorist dangers is biological warfare. A potential means for an enemy to attach a target would be through the dissemination of a biological agent as an aerosol. With this threat to the citizens and military personnel of United States, a mechanism for apt and timely detection of this potential hazard is vital. The current near-real-time detection systems must be placed in the area where the aerosol has contaminated the air. This requires that there be many sampling locations around a specific area in order to have complete coverage.

Most of these detection systems consist of three main components: the inlet, sampler, and the identifier. The inlet draws in the ambient air and has the responsibility of protecting the rest of the device from weather and unwanted debris. The sampling part of a detection system extracts the bioaerosol particles and delivers them to the identifier, which then gives a response to indicate the type of bioaerosol and an indication of its concentration..

The U.S. government is currently developing small and efficient systems for timely and accurate detection of hazardous biological agents. The general requirements for these systems are that they detect bioaerosols in samples extracted from the atmosphere at 100 L/min. The government is funding the Aerosol Technology Laboratory of Texas A&M University to develop inlet systems and concentrators to

---

This thesis follows the style and format of *Aerosol Science and Technology.*

function at this flow rate. For concentration, emphasis is being placed on developing a 100 L/min two-stage virtual impactor that will take in air at the 100 L/min and exhaust a concentrated minor flow air stream at a rate of 1 L/min.

The purpose of this study is to develop the second stage for the concentrator, which will intake air at a nominal flow rate of 10 L/min; and exhaust a minor flow concentrated aerosol stream at 1 L/min. This second stage could also be used with fluorescent optical biological aerosol systems, which would function at 30 L/min. efficiently. The research for this program is being conducted at the Aerosol Technology Laboratory (ATL) and the Applied Research Laboratory (ARL).

Concentrators in a Bioaerosol Detection System

The identifiers in the current bioaerosol detection system typically have a low resolution requiring a large concentration of the biological agents. However the concentration of these agents, once released, is generally very low. This requires evaluation of the bioaerosol particles in large volumes of air, which in turn requires concentrating the particles before collection or analysis. A virtual impactor is one such device for aerosol concentration where excess air is removed from the aerosol. Virtual impactors use the drag force on aerosol particles to achieve the concentration. The major portion (typically 90%) of air in a sampled stream is forced to make a 90° bend, while a minor portion (typically 10%) of air continues in a straight line. The majority of smaller particles follow the major air stream, while the larger particles are transported with the minor flow.

With reference to Figure 1 the sampled air travels through the entrance of the impactor into an acceleration nozzle which accelerates the air stream. Once the sampled

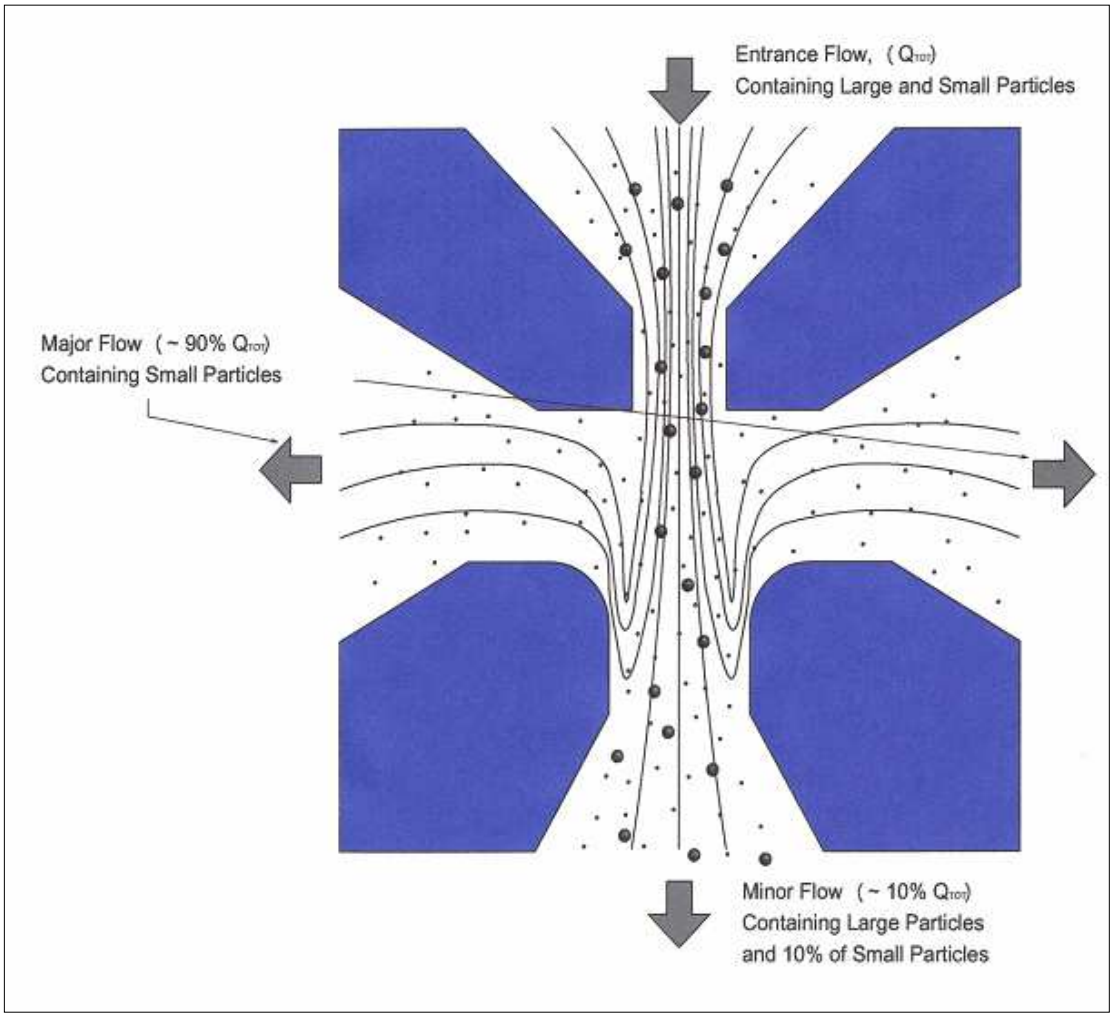

Figure 1: Schematic illustrating the mechanisms behind virtual impaction

air passes the accelerator nozzle, 90% of the total flow rate that entered the virtual impactor makes the 90° bend. The larger particles continue into the minor flow region while the remaining 10% of the original flow transports the concentrated particles from the fractionation stage to perhaps a second stage concentrator. In theory using this ratio of 10:1 total flow to minor flow will achieve a 10X particle concentration for the larger

particle sizes. However, the minor flow exhaust stream also contains a 1X concentration of small particles.

Use of a second stage of virtual impaction will allow an even higher concentration of large particles to be obtained. Such a device is called a two-stage virtual impactor. Once the original sampled air has been through a two-stage virtual impactor the resulting minor flow will ideally have a 100 to 1 concentration ratio from the sampled air using the 10:1 ratio of total flow to minor flow for each stage of the virtual impaction. For contemporary bioaerosol detectors, a concentration factor of 100X is considered sufficient.

THEORY

The most important characteristic of a virtual impactor is its particle penetration, also known as the transmission efficiency (*TE*).

$$TE = \frac{C_m}{C_\infty} \qquad [1]$$

where: C_m = Concentration of aerosol of a particular diameter (D_p) in the minor flow and C_∞ = Concentration of aerosol of a particular diameter in the ambient air.

The Stokes number is a non-dimensional parameter that is used to characterize the ratio of the intertial force to the drag force on a particle. The penetration efficiency of a virtual impactor is a function of the Stokes number.

$$Stk = \frac{\rho_p D_p^2 C_c U_0}{18 \mu L_c} \qquad [2]$$

where: ρ_p = Particle density, D_p = Particle diameter, C_c = The Cunningham correction factor (for particle slip), U_0 = Mean velocity at the accelerator nozzle exit, μ = Fluid viscosity, L_c = Critical dimension (for *Stk* it is half the accelerator nozzle width [$w/2$] and for *Re* it is full width [w]).

The Stokes number can also be considered to be the ratio of the particle stopping distance at the mean velocity of air at the acceleration nozzle exit plane to the accelerator nozzle nozzle width. The stopping distance of a particle is defined as the distance a particle travels given an initial velocity in stagnant (velocity equal to zero) air. For *Stk* << 1 particles will closely follow the curvature of flow streamlines as the drag forces are able to overcome the particle's momentum. Conversely, for *Stk* >> 1 the particles do not

follow curvatures in the streamlines because the momentum of the particles will dominate their behavior.

The Reynolds number (*Re*) is used to characterize the gas phase flow; its value can affect performance of the virtual impactor.

$$\mathrm{Re} = \frac{\rho_f U_0 L_c}{\mu} \qquad [3]$$

where: ρ_f = Fluid density

The Reynolds number is the ratio of viscous forces to inertial forces in the fluid flow. It is commonly used to predict the onset of turbulence in a fluid flow. The CSVI is designed to operate in the laminar flow regime, at Reynolds numbers under 2000.

Previous studies have found acoustic resonance in virtual impactors, which is a manifestation of flow instabilities (Haglund 2003). The acoustic resonance identified by Haglund was a loud "ringing" sound that had a large negative impact on concentrator performance. The onset of turbulent flow can also increase wall losses in virtual impactors. Ding and Koutrakis (2000) found Reynolds above 700 greatly increased wall losses in a linear slot virtual impactor.

The sizes of the particles concentrated by a virtual impactor are partially described by its cutpoint (Stk_{50}). The cutpoint is defined as the particle Stokes number at which 50% of the particles that enter the virtual impactor, are transmitted through the minor flow passage. Ideally, particles with sizes below the cutpoint are exhausted through the major flow passages and particles with sizes larger than Stk_{50} are discharged with the minor flow. Also, ideally particle penetration for the minor flow should be 100% for particles above the cutpoint. However, in reality, some particles will be lost on the internal walls of the concentrator, which degrades the performance.

A virtual impactor's dynamic range (R) is another important performance characteristic.

$$R = \frac{Stk_{90_{UB}}}{Stk_{90_{LB}}} \quad [4]$$

where: $Stk_{90_{UB}}$ = Upper bound Stokes 90, the Stokes number where the transmission efficiency drops off from 90%, $Stk_{90_{LB}}$ = Lower bound Stokes 90, the Stokes number where the penetration first reaches 90%.

At large Stokes number the penetration efficiency of a typical virtual impactor starts to drop due to large particles that cross over the centerline of the critical zone and are lost on the walls of the CSVI. The crossing trajectories effect limits the upper bounds of the high efficiency range (above 90%) of the virtual impactor.

The ideal power ($\dot{W}_{Ideal}$) needed to drive a virtual impactor is dependent on the flow rates through the minor and major flow passages and the pressure drop across the two flow paths:

$$\dot{W}_{Ideal} = \sum Q_i \Delta P_i \quad [5]$$

where: Q_i = The flow rate through flow passage of the CSVI, and ΔP_i = Pressure drop across flow passage in the CSVI.

The pressure drop was measured across the two major flows and the minor flow to determine the ideal power consumption:

$$\dot{W}_{Ideal} = Q_{maj} \Delta P_{maj} + Q_{\min} \Delta P_{\min} \quad [6]$$

where: Q_{maj} = The flow rate through the major flow passages, $Q_{\min}$ = The flow rate through the minor flow passage, ΔP_{maj} = The average pressure drop across the major flow passages, $\Delta P_{\min}$ = Pressure drop across the minor flow passage.

For virtual impactors the pressure drop is a function of the accelerator throat velocity.

$$\Delta P_i = K_i \frac{\rho_f U_0^2}{2} \qquad [7]$$

where: K_i = The pressure loss coefficient for a passage in the CSVI.

Substituting Equation [7] into Equation [5] yields:

$$\dot{W}_{Ideal} = QK \frac{\rho_f U_0^2}{2} \qquad [8]$$

If we rearrange Equation [2] in terms of the velocity, Equation [9] is obtained.

$$U_0 = \frac{9\,(Stk)\mu w}{\rho_p D_p^2 C_c} \qquad [9]$$

Substituting Equation [9] into Equation [8] renders:

$$\dot{W}_{Ideal} = QK \frac{81 Stk^2 (\mu w)^2 \rho_f}{2\left(\rho_p D_p^2 C_c\right)} \qquad [10]$$

For a constant Stokes number and flow rate, the power consumption for a similar performance is proportional to the accelerator slot width squared.

$$\dot{W}_{Ideal} \propto w^2 \qquad [11]$$

The power of the virtual impactors considered herein should be minimal to make the units compatible with battery operation. The limitations on reducing the slot width are determined primarily by manufacturing capability. As the slot width is reduced the

tolerances in the misalignment between the accelerator jet and the receiver gap become critical and harder to hold within an acceptable range. For round jet impactors, Loo and Cork (1988) suggest this misalignment to be a maximum of 5%.

LITERATURE REVIEW

Conventional particle impaction has been utilized by scientists and engineers for decades. The first use of particle impaction occurred in the 1860's by scientists who were studying the relationship between dust and disease. The mechanism of particle impaction allowed them to quickly and effectively collect particles on a glass slide to be examined under a microscope. This method remained relatively unchanged until the latter half of the 20th century (Marple 2004).

Considerable research has been done over the last 40 years in the area of virtual impaction. The concept of virtual impaction was first introduced by Hounan and Sherwood (1965). This eliminated many of the problems associated with inertial impaction by removing the impacting surface. Most important to bioaerosol sampling, this allowed the particles to remain in the aerosol state subsequent to concentration. Understanding of the behavior of virtual impactors has been advanced by many theoretical studies. The understanding of how to predict the characteristics of a virtual impactor was improved by Ravenhall et al. (1978, 1981) who made theoretical predictions for the operating characteristics of a two-dimensional virtual impactor using potential flow and Navier-Stokes equations. These studies confirm the importance of geometrical features in the fractionation zone. Chen, Cheng, and Yeh (1985) further studied virtual impactor behavior by exploring the effects of nozzle Reynolds number and the ratio of the minor flow to the total flow in a nozzle virtual impactor. It was found that the cutpoint for a particular virtual impactor was unaffected by changes in the Reynolds number from 1000 to 8000 and a receiver to nozzle ratio of 1.2 to 1.5. However the cutpoint was much more sensitive to the ratio of the minor flow to the total flow. Chen

and Yeh (1987) expanded on this research by exploring how different geometries influence wall losses in the fractionation zone. The study focused on the receiver geometry and found that selection of receiver geometries has a significant effect on the wall losses. Loo and Cork (1988) investigated the effect of design and operational parameters on the performance characteristics of a circular jet virtual impactor. In their studies the geometrical parameters and flow conditions in the fractionation zone were altered to understand the virtual impactor's sensitivity to these characteristics. Romay et al. (2002) designed a multi-circular nozzle VI for the purpose of biological concentration. Concentration factors of 150-270 were obtained with the virtual impactor used in their study.

Along with experimentation research there have been investigations on the effectiveness of using numerical models to predict the performance of a virtual impactor. A counter-flow virtual impactor was modeled mathematically using potential flow equations and creating particle projections by Lin and Heintzenberg (1995). Asgharian and Godo (1997) calculated particle losses mathematically in a virtual impactor designed by Chen and Yeh (1987) and Chein and Lundgren (1993). In this study flow field information was calculated using finite element analysis and used in the governing equation of spherical particles and fibers to obtain the transport losses in the virtual impactor. Their results agreed with the experimental results.

Linear slot nozzle virtual impactors (LSVI) have also been the target of much research. Sioutas et al. (1994) reported development of an LSVI with a cutpoint below 0.25 μm. Ding and Koutrakis (2000) developed and tested a high volume LSVI that was intended to be used for coarse particle concentration. A variety of geometrical and flow

parameters were studied. It was found that with wider slots the losses of fine particles increased while the penetration for large particles remained constant. A high flow rate four-stage LSVI was studied by Haglund (2003). The sampling flow rate was 1000 L/min and the collection exhaust was 1 L/min. A maximum penetration of 78% was experienced at particle diameter of 3.9 μm AD. A high flow rate three-stage LSVI was studied by Conerly (2004). In this study it was found that a majority of the particle losses occurred at the ends of the slits of the impactor. Seshadri et al. (2005) studied the performance of an LSVI at high mass loading. It was found that for mass loading below 600 μg/l the LSVI remained functional, while at a mass loading of >1000 μg/l the device malfunctioned due to clogging.

Directly applicable to this study is the work of Haglund (2003) and Haglund and McFarland (2004) who were the first to conduct experiments on a circumferential slot virtual impactor (CSVI). In their research, different nozzle configurations were developed and tested. By essentially bending an LSVI slot into a circle, the slot ends were eliminated along with the end effect particle losses reproted by Conerly (2004). The overall dimensions of the device were also reduced. Successful numerical modeling of a CSVI was done by Hari (2003) in order to optimize the CSVI nozzle geometry. Hari's results agreed well with Haglund's experimental results when implementing the same nozzle design. Isaguirre (2004) studied a 100 L/min tandem two-stage CSVI in which the minor flow (flow rate of 10 L/min) of the first stage was drawn into the second stage. His design achieved a maximum efficiency of 95% with a dynamic range of 10. Based on the numerical and experimental work a new CSVI was developed. Prototype units were manufactured by TSI Inc of Shoreview, MN and these are the subject of this

study. The focus of this study is a CSVI with a nominal flow rate of 10 L/min, which is intended for the application of biological concentration. Goals for the development effort are that the CSVI should have a penetration greater than 90% for particles above the cutpoint and have a dynamic range greater than that of previous designs. In addition, the pressure drop should be less than 250 kPa (1-inch of water).

DESIGN

The geometric features of the fractionation zone of the CSVI were based on numerical models run by Hari, Hu, and Seshadri[1]. The main focus of the study was to increase the dynamic range of the CSVI while maintaining flow stability. The fractionation zone design is an upgrade to the second stage units studied by Isaguirre (2004). The major geometrical changes occurred in the accelerator nozzle and the receiver regions. The accelerator nozzle was modified from a chamfered inlet to a parabolic inlet. This allows for better particle alignment of larger particles into the fractionation zone than the radial inlet, thereby allowing for increase penetration of larger particles. Also the receiver section was changed from a sudden expansion to a gradually expanding diffuser which aids in the stability of the flow.

The CSVI was designed to operate at a total flow of 10 l/min with a minor flow of 1 l/min, rendering a 10X concentration factor. In order to accommodate larger particles the fractionation zone diameter had to be increased to 15.2 mm (0.6 in) from the 7.6 mm (0.3 in.) used in Isaguirre's second stage CSVI.. In turn, to keep the same $Stk_{50,}$ the accelerator nozzle had to be reduced from 0.51mm (0.020 in.) to 0.36mm (0.014 in.). Pictures of the CSVI can be seen in Figures 2 and 3.

[1] See Acknowledgements section for mention of their contribution.

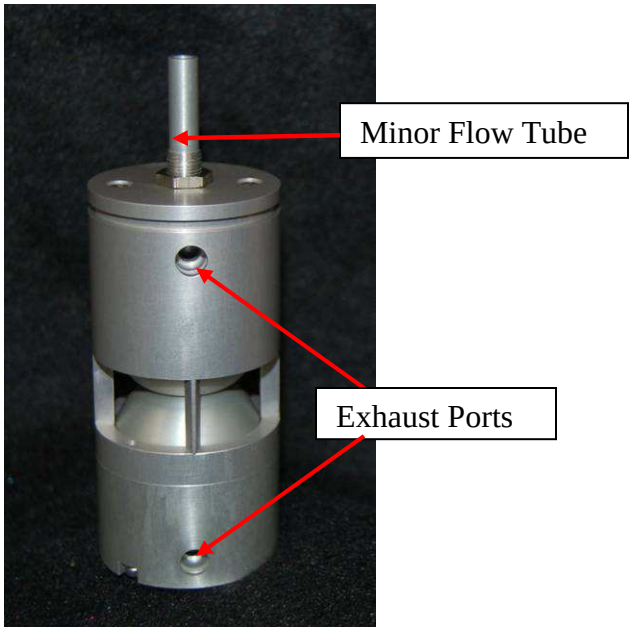

Figure 2: Photograph of the CSVI

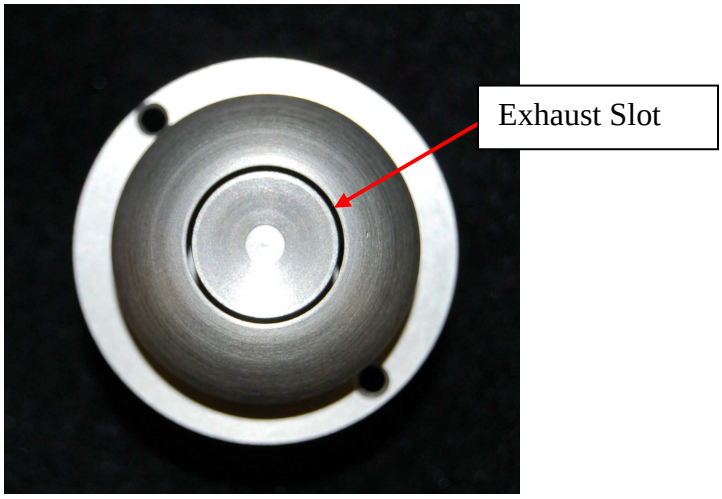

Figure 3: Inside the CSVI

METHODOLOGY

There are three main experimental procedures that are to be used to obtain the data needed to demonstrate achievement of the goals. These are:

1. Measurement of critical dimensions
2. Characterization of aerosol sampling performance
    a. Particle generation
    b. Particle collection
    c. Particle concentration Analysis
3. Pressure measurements

Measurement of the Second Stage CSVI Dimensions

To obtain measurements that will be useful in assessing compliance of dimensions with design criteria, an accuracy of ± 0.0127 mm (0.0005 in.) is necessary. With the configuration of the fractionation zone there is not a way to measure the dimensions directly with that level of accuracy. Instead a mold of the fractionation zone is made by using a two part metrology grade rubber compound (Reprorubber®, Flexbar Machine Corp., Islandia, NY). The CSVI is prepared for measurement by unbolting the two halves to open the unit, and then the accelerator nozzle and receiver blades are cleaned with isopropyl and water. Two components of the rubber are then mixed together in equal amounts. Once completely mixed the compound is then placed in the fractionation zone in each of the two CSVI halves. The two CSVI halves are then reassembled, which forces the rubber compound into the acceleration nozzle, receiver nozzle, and major flow ports. After 15 minutes the rubber compound hardens and the two

CSVI halves are unbolted and reopened. The rubber compound is then removed from the unit leaving a precise mold, which is then sliced using a razor blade perpendicular to the acceleration nozzle slot in section that are approximately 2 mm thick using a standard razor blade. The slice is then viewed under a microscope (Ellipse E600, Nikon, Tokyo, Japan) at a magnification of 20-40X. An attached digital camera (CoolSNAP, Photometrics, Tuscon, AZ) is then used to obtain a photomicrograph of the mold. Figure 4 shows an example of one such picture from an earlier version of the CSVI.

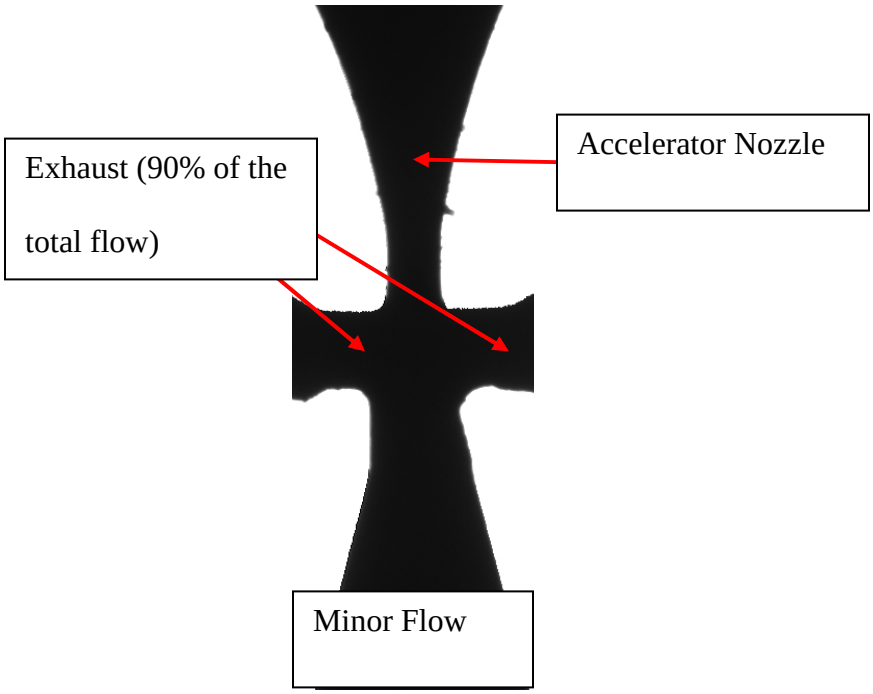

Figure 4: Digital image of the fractionation zone of the CSVI

The dimensions are obtained from the picture using a computer program (Metamorph, Universal Imaging Corp., Downingtown, PA) that has pixel measuring capabilities. The pixels can then be converted to a length scale. The conversion is obtained by photographing and measuring an NIST traceable stage micrometer (KR-851-

C, Klarmann Rulings Inc., Litchfield, NH) at the same magnification and resolution as the photograph of the fractionation zone cross-section mold.

Aerosol Testing

The general procedure for aerosol experimentation is to generate monodisperse aerosols (aerosols comprised of particles that are all the same diameter) and sample the aerosol with the CSVI for a predetermined amount of time. The aerosols in the exhaust and minor flow air streams are then collected. The CSVI is then removed from the flow stream and replaced with a filter that collects all the particles in the inlet air stream for the same amount of time to provide a reference. The penetration efficiency is based on the ratio of the amount of particulate matter collected from the CSVI minor flow exhaust stream to the amount of material collected by the reference filter. The wall loss ratio is based on the difference between the aerosol particles collected by the reference filter with that collected from the major and minor exhaust flows, as a fraction of the amount of material in the reference sample.

Particle Generation

Two methods of aerosol generation are to be used in the experimentation. The first method utilizes a six-jet Collison nebulizer (CN311, 6 Jet BGI Inc., Waltham, MA) to aerosolize solid monodisperse polystyrene spheres (PSL) (Duke Scientific, Palo Alto, CA). This is method is used for the particle size range of 0.5 µm to 2.0 µm diameter. A suspension of PSL in water is created and stored in a glass sealed jar. The concentration of the suspension is kept less than about 10^9 particles/mL, which is the limit above which the Collison nebulizer produces an unacceptable level of doublets (two

particles bound together, which result from there being two PSL beads in one spray droplet) (May 1973). Generally, enough of the master solution is made in order to run multiple tests with the same concentration of PSL in the solution.

The Collison nebulizer is then filled with 60 mL of the PSL solution and pressurized air at 103-207 Pa (15-30 psig) is passed into the device. During an experiment a magnetic bead is used stir the PSL to keep it from settling in the master solution. To ensure that the PSL to water concentration in the Collison remains close to that of the master solution, the Collison is emptied into a second glass container at the conclusion of each trial during an experiment. This suspension could then be reused in another set of experiments as the master solution.

For the large particles (2.0 µm to 20 µm) a vibrating orifice aerosol generator, VOAG, (Model 3450, TSI Inc., Shoreview, MN) was employed. The VOAG generates liquid droplets from a solution containing ethanol, oleic acid, and an analytical tracer, fluorescein. After generation of the droplets the solvent (ethanol) evaporates leaving residual monodisperse liquid spheres, which are the particles of interest. The master solution is made of 90% ethanol, 9% oleic acid, and 1% fluorescein by volume. The master solution is diluted to achieve the various particle sizes. The diameter of droplets generated by the VOAG can be calculated from the following relationship:

$$D_p = \left(\frac{6 Q_{VOAG} C_{vol}}{\pi f_{VOAG}} \right)^{1/3} \qquad C_{vol} = \frac{x_{fr} V_m}{V_m + V_d} \qquad [12]$$

where: D_p = Particle diameter, Q_{VOAG} = Solution volumetric flow rate (parameter set on VOAG), C_{vol} = Volume fraction of oleic acid and fluorescein, f_{VOAG} = Vibrating

orifice frequency (parameter set on VOAG), x_{fr} = Fraction of ethanol in master solution, V_m = Volume of master solution, V_d = Volume of dilution ethanol.

Generally, 100 mL of ethanol is poured into a mixing container and the necessary volume of the master solution is added to the ethanol using a pipette (2000 Reference Series, Eppendorf AG, Hamburg, Germany). When the solution has been mixed it is then put into the syringe pump of the VOAG. The VOAG is then operated according to the manufacturer's instructions, with the main focus on producing monodisperse particles. Fine tuning is achieved by adjusting the excitation frequency of a piezo-ceramic that drives the vibrating orifice. To achieve this, an adapter is used to turn the dispersion air and blow it toward the aerosol stream exiting the orifice. If the particles are not monodisperse, multiple streams will be seen above the point where the air makes contact with the orifice output. Once the excitation frequency is properly adjusted only one stream will be observed. At this point monodispersity is confirmed with an Aerosol Particle Sizer (APS) (Model 3321, TSI Inc, St. Paul, MN).

To measure the particle size that is generated using the VOAG, the particles are impacted onto a glass microscope slide. The particles are magnified 400X with a microscope and then photographed using the same microscope and camera that are discussed in the measurement procedure section. They are measured using the Metamorph program that measures the pixels and the pixels are then converted to a unit of length using the calibration obtained from measuring a stage micrometer under the same magnification. A flattening factor of 1.29 is used to observe the droplet size (diameter of an oblate spheroid) to the actual droplet diameter. (Thien, 2004).

Particle Sampling and Collection

Once the aerosol is generated, it is then drawn through the CSVI by a blower. Figure 5 gives a schematic of the test fixture used in testing the CSVI.

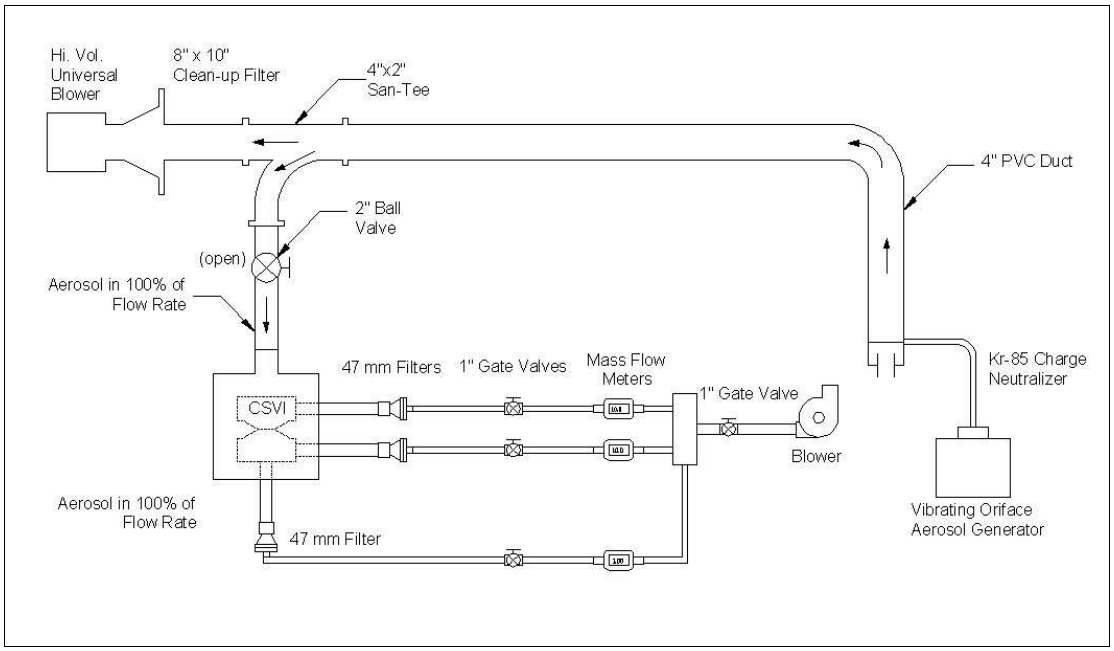

Figure 5: Schematic of the complete flow system for the CSVI aerosol testing

A schematic of an aerosol plenum, in which the CSVI was mounted during the tests, is presented in Figure 6. The effectiveness of a similar plenum design was tested

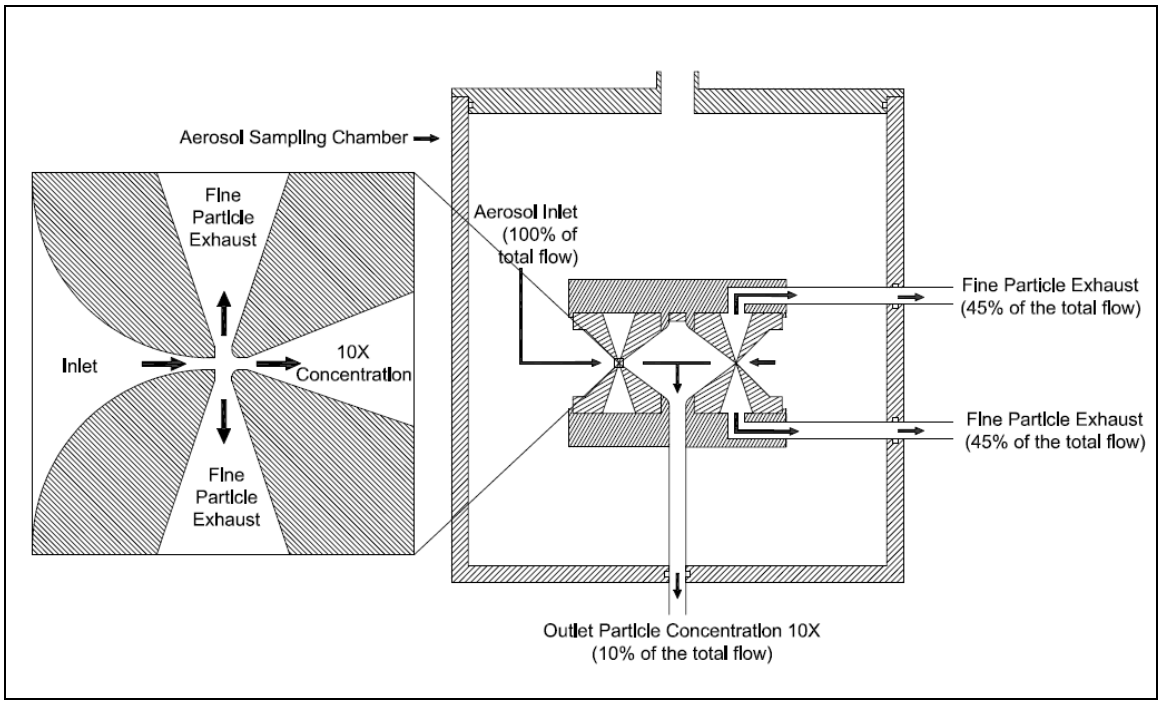

Figure 6: Schematic of the plenum used during aerosol sampling of the CSVI during experimentation

by Isaguirre (2004) and no significant losses to particles, prior to entering the CSVI, were found.

The flow rates are measured using calibrated mass flow meters (Model 4045, TSI Inc, St. Paul, MN) and controlled using standard gate valves. Particle samples are then collected from the major and minor air flow exhausts of the CSVI and from the inlet air stream (reference) on glass fiber filters (Type A/D glass fiber filters, Pall Corp., East Hills, NY). The CSVI is run for a predetermined length of time -- normally ten minutes permits collection of sufficient particulate matter for the analyses. The second stage CSVI is then removed and the reference filter is installed. The air stream containing the same concentration of aerosol, which was sampled by CSVI, is then run through the reference filter at the same total flow rate for the same duration. This gives an entity that

represents the total amount of particulate matter that entered the CSVI and can be compared to the particles that are collected in the minor flow to give the penetration and in the total of the minor and major flows to give wall losses.

The filters are then placed separately into 125 ml glass containers and the fluorescein is eluted in a solvent, i.e., the particles are dissolved extract the analytical tracer contained in the particles. The filters containing PSL are soaked in 10-20 ml of ethyl acetate for a minimum of 1 hour. The liquid particles generated by the VOAG are soaked in 20-40 ml of a solution containing 50% isopropyl and 50% water and are soaked for a minimum of 6 hours. Care is taken to ensure that the same amount of solution is used to elute the particulate matter so that direct comparisons can be made.

Particle Concentration Analysis

Once the filters have soaked for the necessary time, about 6-7 ml of each solution is put into 12 × 75 mm glass cuvettes so the solutions can be analyzed in a fluorometer (FM109515, Barnstead International, Dubuque, IA), which provided data on the relative concentration of fluorescent tracers in the solutions. Three colors of PSL are used (red, blue, and green), for the three sizes of PLS used in the testing. These tracers emit light when excited by certain shorter wavelengths of light. The light, emitted from the tracers, is first passed through appropriate high-pass optical filters and then the intensity is measured with the fluorometer. In addition to the high-pass filters, the fluorometer also employs a low pass filter on the excitation light, which removes wave lengths that may interfere with the analysis from the spectrum. The high-pass filters are selected to allow the three PSL colors to be analyzed in the same solution, which, in turn, allows testing of three PSL particle diameters during one test.

Each sample solution's light emission intensity is recorded from a digital readout on the fluorometer. The minor flow collection is then compared to the reference collection to obtain transmission efficiency. This is done for all the particle sizes (0.5 µm to 20 µm) and the results are plotted on a graph depicting the transmission efficiency as a function of Stokes number.

Pressure Drop Measurements

The same test setup used to draw the air containing aerosol through the CSVI is used to measure the pressure drop across the major and minor flow passages at different flow rates. Air is drawn through the CSVI with a vacuum pump. The pressure differential is then measured with an inclined monometer (Durablock, Dwyer Instruments Inc., Michigan City, IN) attached to each of the exits of the exhaust ports and the exit of the minor flow port. The data collected are presented on a plot of pressure drop as a function of flow rate.

Using Equation [7], the pressure coefficients were also found for the CSVI at the various flow rates tested. The data for the pressure coefficients are presented on a plot of the pressure coefficient as a function of the Reynolds Number.

UNCERTAINTY ANALYSIS

There are two calculations that affect the results obtained: the Stokes Number calculation and the efficiency calculations. First, consider the uncertainty in the Stokes number.

$$\delta R = \left[\sum_{i=1}^{n} \left(\frac{\partial R}{\partial X_i} \delta X_i \right)^2 \right]^{\frac{1}{2}} \quad [13]$$

where: δR = Uncertainty value associated with calculation R, X_i = Variable used in the calculation of R, δX_i = Uncertainty associated with the variable X_i

There are two calculations that affect the results obtained: the Stokes Number calculation and the efficiency calculations. The first uncertainty calculation is the Stokes number.

Substituting:

$$U_0 = \frac{Q}{2 w \pi D_c} \quad [14]$$

and

$$C_c = 1 + 2.52 \frac{\lambda}{D_p} \quad [15]$$

into Equation [2] gives the Stokes number in terms of the experimental parameters.

$$Stk = \frac{\rho_p D_p^2 Q \left(1 + 2.52 \frac{\lambda}{D_p} \right)}{18 \pi \mu w^2 D_c} \quad [16]$$

where: λ = mean free path of air, D_c = fractionation zone diameter.

The parameters that were measured are the flow rate (Q), accelerator nozzle width (w), diameter of the fractionation zone (D_c), and the particle diameter (D_p). The other values, such as particle density and the mean free path of air, are results from tabulated values and the error with these values is assumed to be of no consequence. Using the Kline-McClintock method the calculation for the error in the Stokes number is as follows:

$$\frac{\partial Stk}{\partial Q} = \frac{Stk}{Q} \qquad [17]$$

$$\frac{\partial Stk}{\partial w} = \frac{-2Stk}{w} \qquad [18]$$

$$\frac{\partial Stk}{\partial D_c} = \frac{-Stk}{D_c} \qquad [19]$$

$$\frac{\partial Stk}{\partial D_p} = \frac{Stk}{D_p}\left[\frac{2D_p + 2.52\lambda}{D_p + 2.52\lambda}\right] \qquad [20]$$

Therefore the uncertainty of the Stokes number calculation is:

$$\delta Stk = Stk\left[\left(\frac{\delta Q}{Q}\right)^2 + \left(\frac{-2\delta w}{w}\right)^2 + \left(\frac{-\delta D_c}{D_c}\right)^2 + \left(\frac{\delta D_p}{D_p}\left\{\frac{2D_p + 2.52\lambda}{D_p + 2.52\lambda}\right\}\right)^2\right]^{\frac{1}{2}} \qquad [21]$$

The estimated values of uncertainties for Q, w, D_c, D_p are given in Table 1.

Table 1: Uncertainties associated with experimental measurements

Measured Parameter	Uncertainty [%]
Accelerator width [w]	0.25%
Particle diameter [D_p]	2.0%
Critical zone diameter [D_c]	0.50%
Measured flow rate [Q]	2.0%
Repipeter volume [V_s, V_r]	2.00%

This renders the percent uncertainty for the Stokes calculation:

$$\frac{\delta Stk}{Stk} = \left[(0.02)^2 + (-2 \cdot (0.005))^2 + (-0.005)^2 + \left(0.03 \left\{ \frac{2D_p + 2.52\lambda}{D_p + 2.52\lambda} \right\} \right)^2 \right]^{\frac{1}{2}} \quad [22]$$

Over the particle sizes that the CSVI tested Equation [22] gives a peak error slightly larger than 4.3%. Likewise the uncertainty for the penetration calculation is determined below:

Substituting:

$$C_m = Q_s V_s t_s F_s \quad [23]$$

and

$$C_\infty = Q_r V_r t_r F_r \quad [24]$$

into Equation [1] renders

$$TE_{meas} = \frac{Q_s V_s t_s F_s}{Q_r V_r t_r F_r} \quad [25]$$

where: TE_{meas} = *M*easured particle penetration, Q_s = Flow rate of the CSVI while sampling, V_s = Volume of the solvent used in the sample, t_s = Sampling time for the CSVI, F_s = Fluorometer reading from the sample, Q_r = Flow rate of the reference sample, V_r = Volume of the solvent used in the reference sample, t_r = Sampling time of the reference sample, F_r = Fluorometer reading of the reference sample.

Assuming that the stopwatch used is accurate, the uncertainty of the time is negligible. Using the Kline-McClintock method gives the following equation for the uncertainty of the penetration:

$$\delta TE_{meas} = TE_{meas}\left[\left(\frac{\delta Q_s}{Q_s}\right)^2 + \left(\frac{-\delta Q_r}{Q_r}\right)^2 + \left(\frac{\delta V_s}{V_s}\right)^2 + \left(\frac{-\delta V_r}{V_r}\right)^2 + \left(\frac{\delta F_s}{V_s}\right)^2 + \left(\frac{-\delta F_r}{F_r}\right)^2\right]^{\frac{1}{2}} \quad [26]$$

Looking again at the uncertainty values given in Table 1 and putting them into Equation [26] gives:

$$\frac{\delta TE_{meas}}{TE_{meas}} = \left[(0.02)^2 + (0.02)^2 + (0.001)^2 + (0.001)^2 + \left(\frac{\delta F_s}{V_s}\right)^2 + \left(\frac{-\delta F_r}{F_r}\right)^2\right]^{\frac{1}{2}} \quad [27]$$

The uncertainty of the fluorometer readings varies with each experimental data point. The readings for multiple reference samples, which should be identical, render inconsistencies of up to about 10%. The experimental results render penetration uncertainty calculations that range from 8% to 12%.

RESULTS AND DISCUSSION

Previous virtual impactors obtained high maximum particle penetrations (>95%), but they were unable to achieve the high efficiencies for large ranges in particle sizes. A major limitation was the tendency for larger particles to be impacted either in the fractionation zone or on the walls of the acceleration nozzle because of their crossing trajectories. These particles would enter the fractionation zone at an angle and would not be able to enter the receiver nozzle before impacting on a surface.

Geometric changes to the acceleration and receiver nozzles have been done to achieve a larger range of Stokes numbers (or particle sizes) for which the penetration efficiency is ≥ 90%. These geometrical changes cause the large particles to align with the streamlines of the jet exiting the accelerator, allowing them to enter the receiver section. The results of these changes have allowed particles from 3.8 μm AD to at least 22 μm AD to have above 90% penetration into the minor flow at a total flow rate of 10 lpm. This renders a dynamic range at 10 l/min of at least 39.

The effects on the particle penetration efficiency from unbalanced flows in the major flows was studied. It was found that there was no reduction in performance for major flow imbalances up to 10% for flow rates of 10 and 30 l/min.

Particle Penetration

The particle penetration for the CSVI as a function of the particle diameter for flow rates from 10 to 40 L/min is presented in Figure 7.

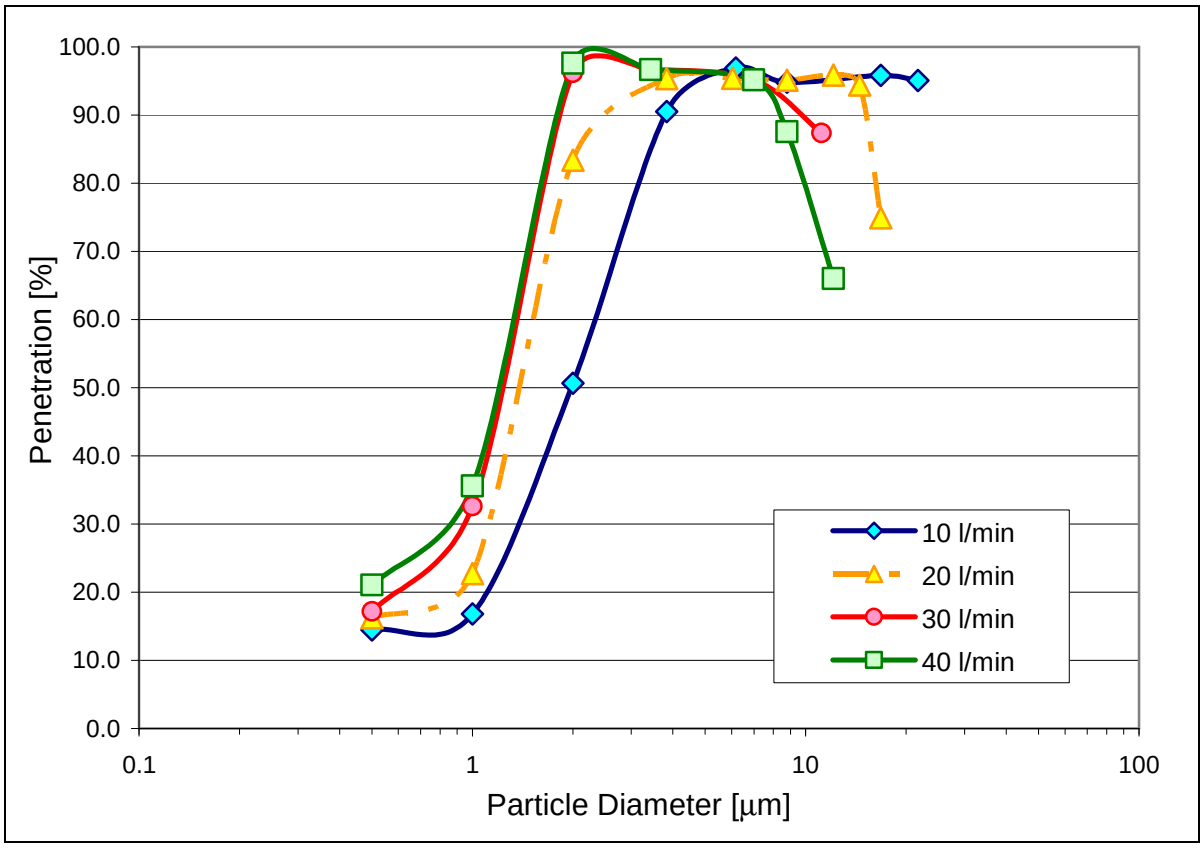

Figure 7: Penetration efficiency as a function of the particle diameter for flow rates of 10 L/min to 40 L/min

The particle cutpoint corresponding to 50% penetration for the four flow rates can be seen in Table 2.

Table 2: Experimentally obtained cutpoints for the CSVI at the tested flow rates

Flow Rate [l/min]	Cutpoint Size (AD) [µm]
10	2.0
20	1.5
30	1.2
40	1.2

The data corresponding to the particle penetration as a function of Stokes number (Figure 8) show the average cutpoint Stokes number for each of the flow rates tested to be 0.85.

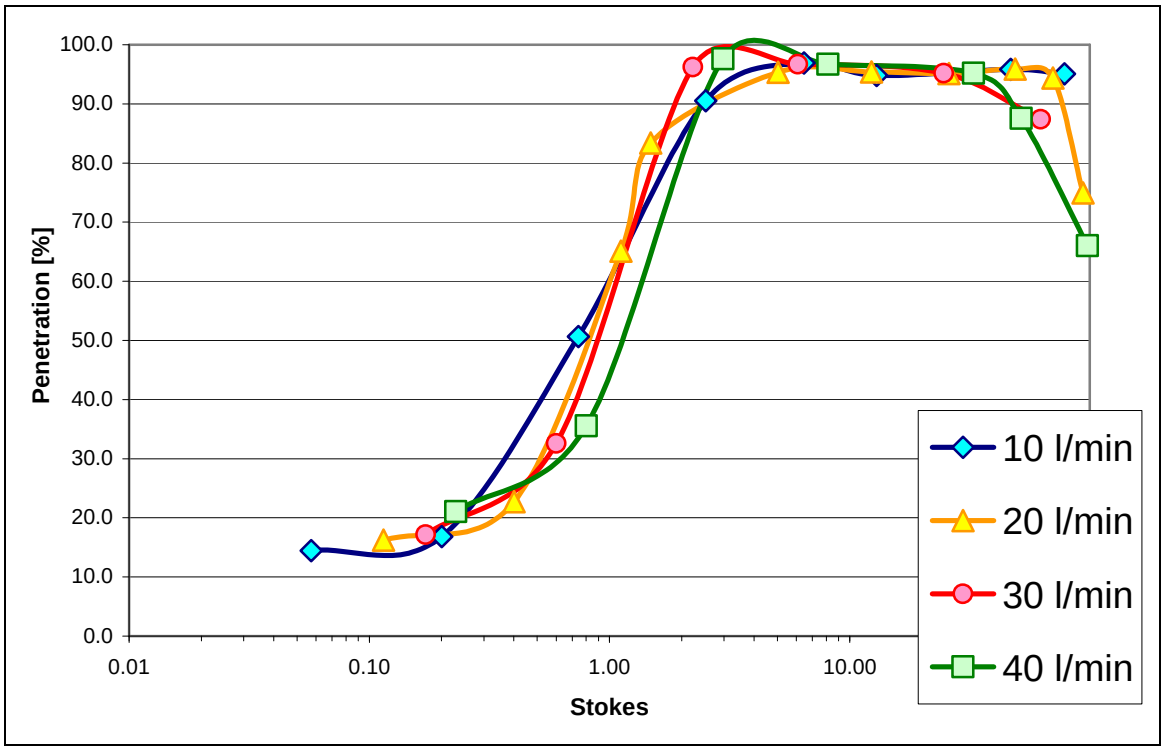

Figure 8: Penetration efficiency as a function of the Stokes number for flow rates of 10 L/min to 40 L/min

These values are comparable to the predicted numerical values from simulation conducted by Hu for the same CSVI .

The dynamic range for the four experimental flow rates is shown in Table 3.

Table 3: Dynamic ranges for the CSVI at flow rates from 10 L/min to 40 L/min

Flow Rate [l/min]	Dynamic Range
10	>39.2[2]
20	52.0
30	47.2
40	40.5

The highest experimentally obtained dynamic range is 52.0[2], which occurs for a flow rate of 20 L/min.

Figure 9 shows the experimental data for particle penetration for the 10 L/min CSVI compared to the numerical results obtained by Shishan Hu. The predicted numerical 50% particle penetration cutpoint is 2.5 μm and the experimental 50% penetration cutpoint is 2.0 μm.

[2] The dynamic range could not be obtained for 10 L/min due to limitation in size of particle generation. If the trend for the other flow rates holds true it is expected that the dynamic range for 10 L/min would be higher than the others.

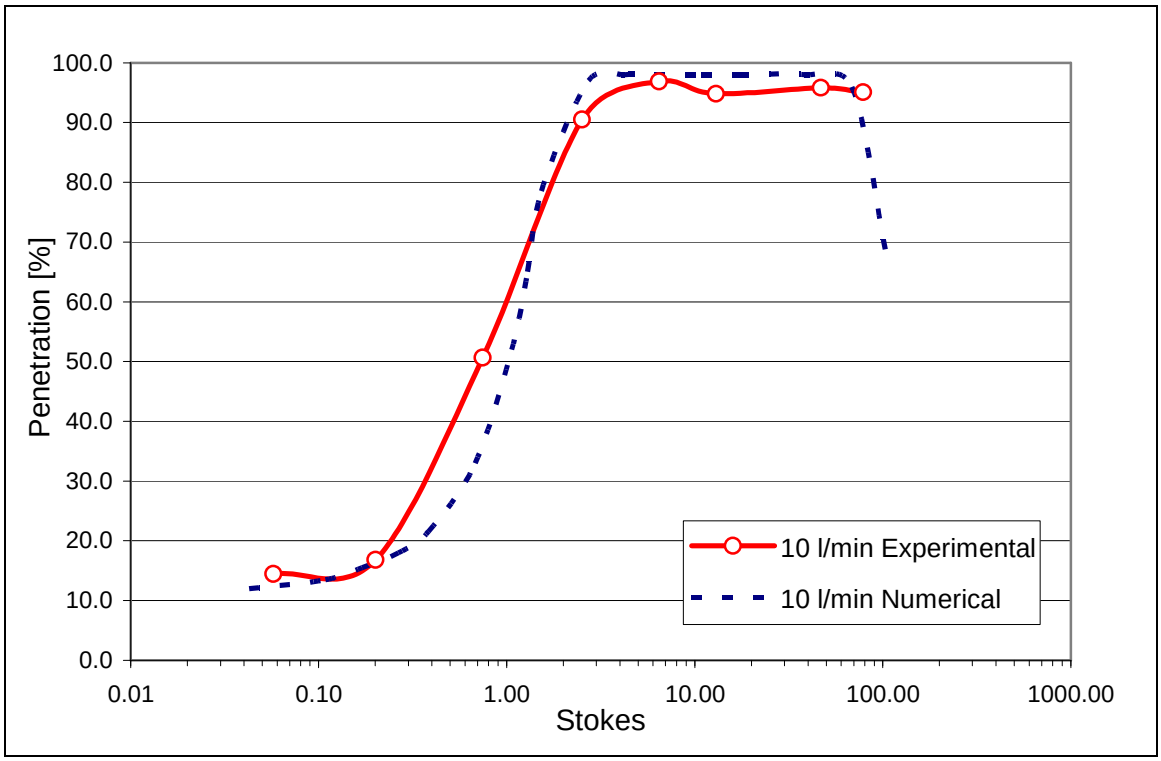

Figure 9: Penetration efficiency as a function of the Stokes number comparing the experimental data to the data obtained by numerical simulations

Total to Minor Flow Ratio

The particle penetration as a function of the Stokes number for flow ratios of 20:1, 10:1, and 5:1 at a total flow rate of 20 L/min can be seen in Figure 10.

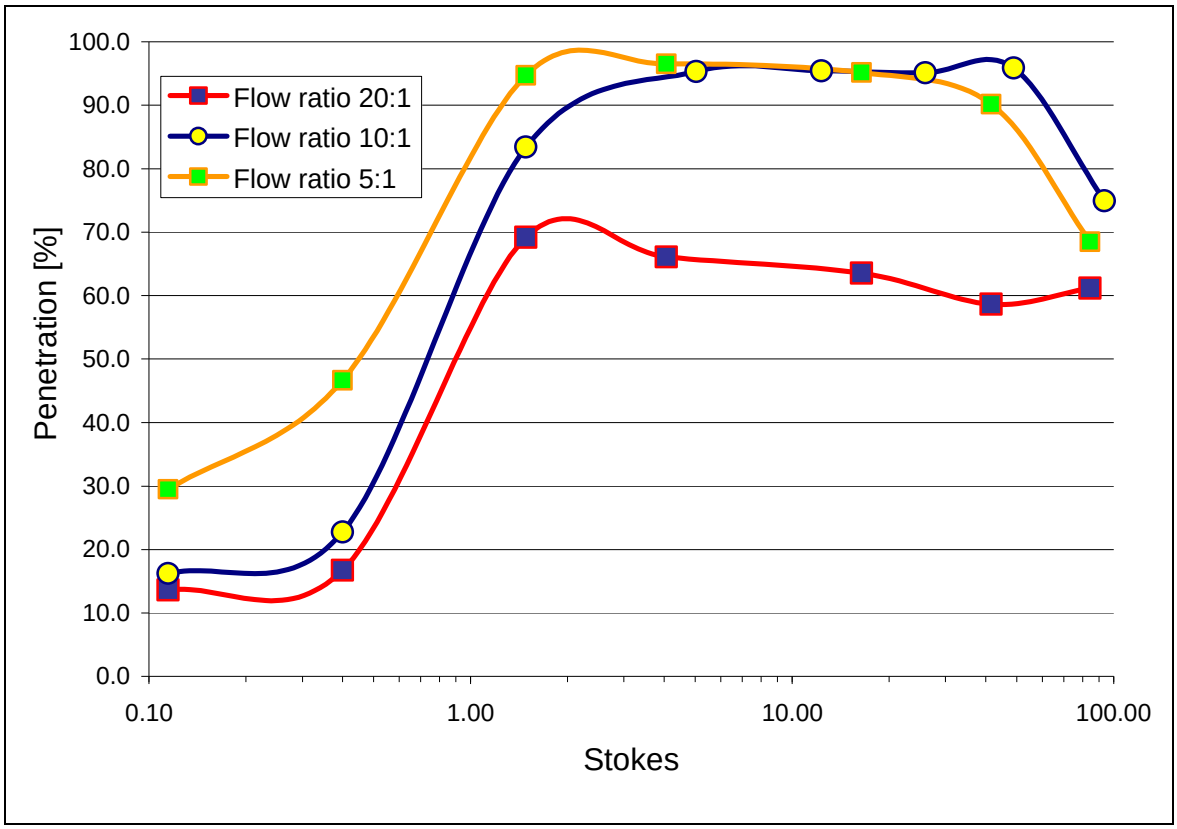

Figure 10: Particle penetration as a function of the Stokes number for flow ratios of 20:1, 10:1, and 5:1 at a total flow rate of 20 L/min

As the ratio of minor flow to total flow increases, the cutpoint decreases. For the ratio of 20:1 the peak collection efficiency is 69%. For the flow ratio of 5:1 the peak penetration efficiency is similar to value of 97% for the nominal flow ratio of 10:1. The penetration efficiency for the 5:1 flow ratio starts to droop at lower values of the Stokes number than occurs with the 10:1 flow ratio.

Major Flow Offset

Another important aspect of the functionality of the CSVI is the ability to perform satisfactorily even with imbalances in the two major flow exhaust streams. In use, the flow rates of air in the two major flow exhaust ports will likely need to be controlled, therefore, it is important to know the allowable variance between the major flows. The particles that will be most affected by these imbalances are the smaller particles that have a penetration efficiency $\geq 90\%$. Flow rates of 10 and 30 l/min were tested with varying major flow imbalance percentages[3] with particles having a Stokes number of approximately 4.5 (5 μm AD for 10 L/min and 3 μm AD for 30 L/min). Figure 11 shows the particle penetration as a function of the major flow imbalance percentages.

[3] The major flow imbalance percentages are defined as the absolute value between the differences in the major flows divided by the total sampling flow rate of the CSVI $\left(\left|Q_{maj1} - Q_{maj2}\right|\right)/Q_{tot}$.

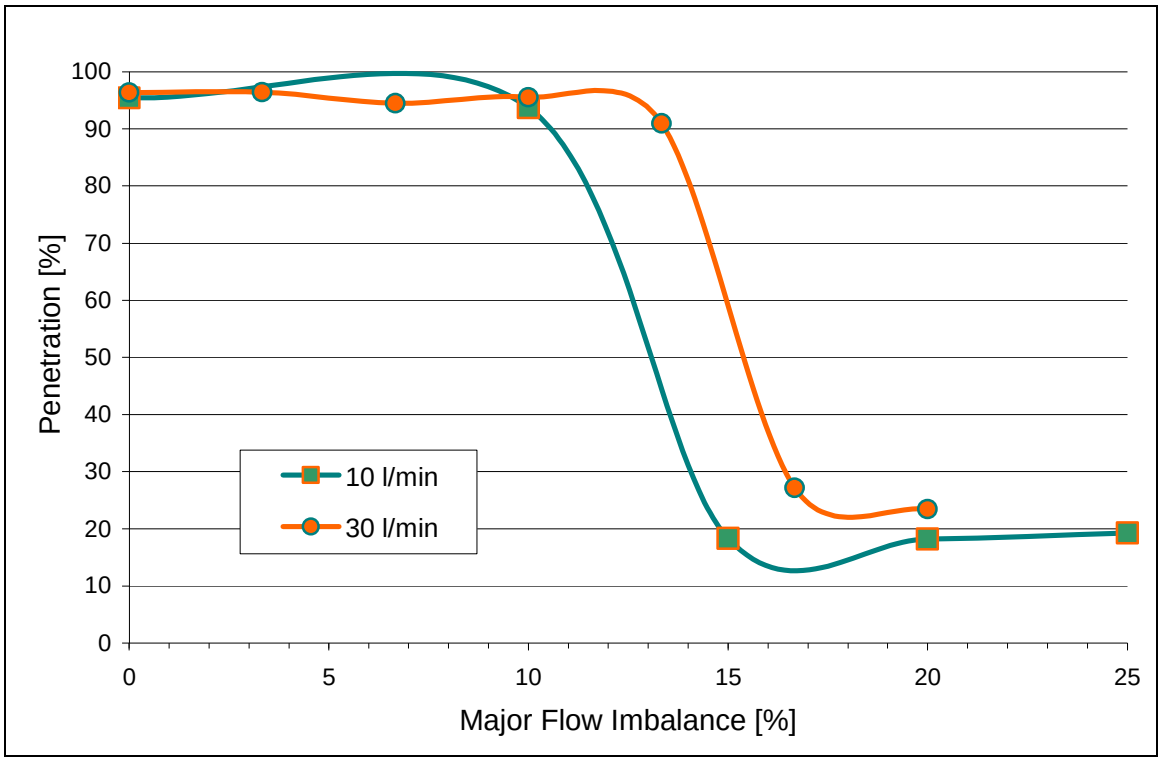

Figure 11: Penetration efficiency as a function of the major flow imbalance percentages

An imbalance of less than 10% has an unnoticeable effect on particle penetration. For instance, for a total flow rate of 10 L/min the difference between the major flow rates can be as much as 1 L/min.

Pressure Drop

One major motivation for using a slot type virtual impactor is the low pressure drop associated with relatively large flow rates. Figure 12 gives the pressure drop across the CSVI as a function of flow rate.

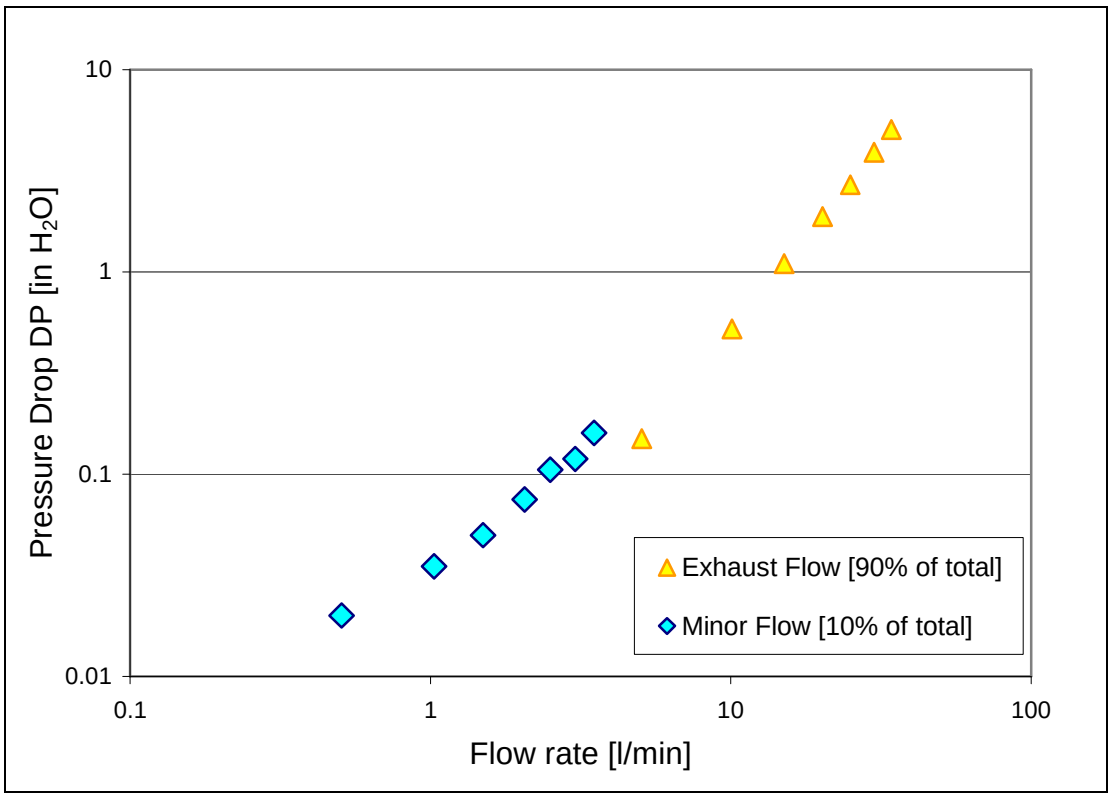

Figure 12: Pressure drop across the exhaust and minor flows of the CSVI at total flow rates from 5 L/min to 33 L/min

The flow was varied from 5 to 33 l/min. The pressure drop across the major flow varied from 37.4 to 1258 Pa (0.15 to 5.05 in. H_2O) and the pressure drop across the minor flow system varied from 5.0 to 39.9 Pa (0.02 to 0.16 in. H_2O). The pressure drop in the minor section is lower due to the lower flow rate through this region. The pressure coefficient as a function of the flow rate number is shown in Figure 13.

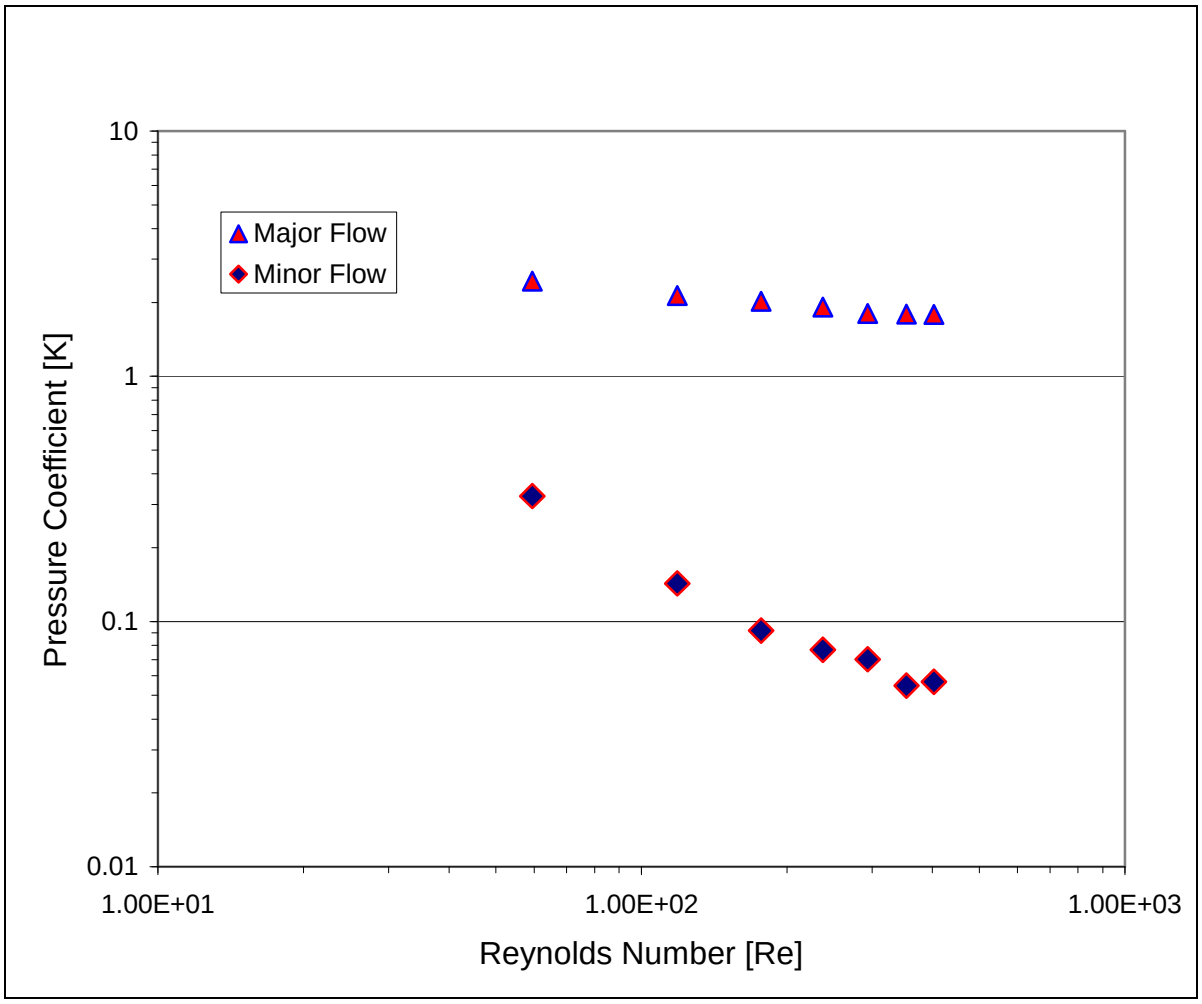

Figure 13: Pressure coefficient for the CSVI as a function of the flow rate

At the lowest flow rate of 5 L/min the pressure coefficient is 2.4. As the flow increases the pressure coefficient asymptotically approaches 1.8. The pressure coefficient for the designed flow rate of 10 L/min is 2.1.

SUMMARY AND CONCLUSION

A circumferential slot virtual impactor was designed and manufactured in order to develop a highly efficient particle concentration device that would interface with current bioaerosol detection equipment. The focus of the study was to test the newly designed fractionation zone. The measured Stk_{50} value was 0.76 corresponding to a 2.0 μm AD particle for the designed flow rate of 10 L/min. The largest particle that was collected in the CSVI at 10 L/min was 22 μm AD rendering the dynamic range of the unit to be significantly higher than previous CSVI's operating at similar cutpoints and pressure drops.

The result of the new geometry was comparable to the results that were rendered numerically. This gives more credibility to the effective use of numerical studies for predicting the performance of virtual impactors.

In conclusion this device performed in a manner that will allow it to be successful used in conjunction with any device that requires a 10X concentration of aerosols with inlet flow rates of 10 to 30 L/min. Specifically this device will work well with current bioaerosol detection devices that are being used by the Aerosol Technology Laboratory.

REFERENCES

Asgharian, B.and Godo, M.N. (1997). Transport and Deposition of Spherical Particles and Fibres in an Improved Virtual Impactor. *Aerosol Science and Technology* 27: 499-506.

Chein, H.and Lundgren, D.A. (1993). A Virtual Impactor with Clean Air Core for the Generation of Aerosols with Narrow Size Distributions. *Aerosol Science and Technology* 18: 376-388.

Chen, B.T. and Yeh, H.C. (1987). An Improved Virtual Impactor. *Journal of Aerosol Science* 18: 203-214.

Chen, B.T., Cheng, Y.S., and Yeh, H.C. (1985). A Novel Virtual Impactor: Calibration and Use. *Journal of Aerosol Science* 16: 343-354.

Conerly, S. (2004). Multi-Stage Linear Slot Virtual Impactor for Concentration of Bioaerosols, M.S. Thesis, Department of Mechanical Engineering, Texas A&M University, College Station, Texas.

Ding, Y. and Koutrakis, P. (2000). Development of a Dichotomous Slit Nozzle Virtual Impactor. *Journal of Aerosol Science* 31(12): 1421-1431.

Haglund, J.S. (2003). Two Linear Slot Virtual Impactors for Concentration of Bioaerosols, Ph.D. Dissertation, Department of Mechanical Engineering, Texas A&M University, College Station, Texas.

Haglund, J.S. and McFarland A.R. (2004). A Circumferential Slot Virtual Impactor. *Aerosol Science and Technology* 38: 664-674.

Hari, S. (2003). Two Computational Fluid Dynamics (CFD) Simulations of Dilute Fluid-Particle Flows, Ph.D. Dissertation, Department of Nuclear Engineering, Texas A&M University, College Station, Texas.

Hounan, R.F. and Sherwood, R.J. (1965). The Cascade Centripeter: A Device for Deterring the Concentration and Size Distribution of Aerosols. *American Industrial Hygiene Association Journal* 2: 122-131.

Isaguirre, R. (2004). A Two-Stage Circumferential Slot Virtual Impactor for Bioaerosol Concentration, M.S. Thesis, Department of Mechanical Engineering, Texas A&M University, College Station, Texas.

Lin, H. and Heintzenberg, J. (1995). A Theoretical Study of the Counterflow Virtual Impactor. *Journal of Aerosol Science* 26(6): 903-914.

Loo, B.W. and Cork, C.P. (1988). Development of High Efficiency Virtual Impactors. *Aerosol Science and Technology* 9: 167-176.

Marple, V. (2004). History of Impactors-The First 110 years. *Aerosol Science and Technology* 38: 247-292.

May, K.R. (1973). The Collison Nebulizer: Description, Performance, and Application. *Journal of Aerosol Science* 4: 235-243.

Ravenhall, D.G., Forney, M., and Jazayeri, L.J. (1978). Aerosol Sizing with a Slotted Virtual Impactor. *Journal of Colloid and Interface Science* 65(1): 108-117.

Ravenhall, D.G., Forney, L.J., and Hubbard, A.L. (1981). Theory and Observation of a Two-Dimensional Virtual Impactor. *Journal of Colloid and Interface Science* 85: 508-520.

Romay, F.J., and Roberts, D.L., et al. (2002). A High Performance Aerosol Concentrator for Biological Agent Detection. *Aerosol Science and Technology* 36: 217-226.

Seshadri, S., Phares, D.J., Kim, T., Kihm, K.D., Smith, D., and McIntyre, P.M. (2005). Performance of a Slit Virtual Impactor Operated at High Particle Mass Loading. *Journal of Aerosol Science*36: 541-547.

Sioutas, C., Koutrakis, P., and Burton, R.M. (1994). Development of a Low Cutpoint Slit Virtual Impactor for Sampling Ambient Fine Particles. *Journal of Aerosol Science*25(7): 1321-1330.

Thien, B. (2004). Flattening Factor for Oleic Acid Particles on Q-slides. Lab Report, Aerosol Technology Laboratory, Department of Mechanical Engineering, Texas A&M University, College Station, Texas.

VITA

Name:	Clinton Wayne Adams
Address:	3570 CR 513 Hamilton, TX 77057
Email Address:	cwa8080@gmail.com
Education:	B.S., Mechanical Engineering, Texas A&M University, 2003 M.S., Mechanical Engineering, Texas A&M University, 2006